Wireless Interference Estimation Using Machine Learning in a Robotic Force-Seeking Scenario

Richard Candell*, Karl Montgomery*, Mohamed Kashef†, Yongkang Liu†
*Intelligent Systems Division †Advanced Network Technologies Division
National Institute of Standards and Technology (NIST)
Gaithersburg, Maryland, United States
Email: {richard.candell, karl.montgomery, mohamed.kashef, yongkang.liu}@nist.gov

Sebti Foufou
Computer Science Department
University of Burgundy
Dijon, France
sfoufou@u-bourgogne.fr

***Abstract*—Cyber-physical systems are systems governed by the laws of physics that are tightly controlled by computer-based algorithms and network-based sensing and actuation. Wireless communication technology is envisioned to play a primary role in conducting the information flows within such systems. A practical industrial wireless use case involving a robot manipulator control system, an integrated wireless force-torque sensor, and a remote vision-based observer is constructed and the performance of the cyber-physical system is examined. By using readings from the remote observer, an estimation system is developed using machine learning regression techniques. We demonstrate the practicality of combining statistical analysis with machine learning to indirectly estimate signal-to-interference of the wireless communication link using measurements from the remote observer. Results from the statistical analysis and the performance of the machine learning system are presented.**

***Index Terms*—industrial wireless, 802.11, factory communications, cyber-physical systems, wireless networking, robotics**

I. Introduction

The advances in wireless devices for cyber-physical systems (CPS) have led to rapid adoption of the industrial wireless system (IWS) in factories. The use cases for IWSs include process monitoring and control, discrete manufacturing, safety systems, and flexible factory work cells [1]. Implementation of wireless systems for industry has many advantages due to the lower cost, ease of scale, and flexibility due to the absence of cabling. However, these advantages come with challenges [2]–[4]. Such challenges include unpredictable latency, error uncertainty, and increased information loss when operating in the presence of significant interference and limited spectral resources [5]. When network operations are impaired by interference, fading, and propagation loss, the physical system performance may also be impaired. These impairments contribute to a change in the quality of information flow between wireless nodes and require careful co-design of the network and controller [6], [7].

Interference presents a significant challenge to IWSs and the underlying physical systems that rely on them. While wireless systems can be designed to support many users and devices and cognitive radio can be useful in scheduling transmissions and avoiding problem locations within the spectrum, sometimes it is not possible to avoid interference entirely or responses to interference is too slow. Sources of interference may be narrowband or wideband in nature. They include multi-path reflections, competing wireless systems, non-communication devices such as microwave ovens and industrial machines, and intentional jamming [8].

Methods to estimate, avoid, or mitigate interference are required for the deployment of reliable and deterministic IWSs. Existing methods rely on traditional signal processing and novel cognitive radio techniques. In [9], a method of desensitizing a 5G cellular network using interference cancellation of transmissions from neighboring cells is presented. Interference cancellation equipment is highly complex and costly, and the impact to latency in a CPS must be well understood. In [10], a method using a dedicated link quality estimation (LQE) node using received signal strength and information (RSSI) obtained from received data packets to identify interference and multi-path is presented as a viable approach to LQE in IEEE 802.15.4 networks without introducing additional traffic. In [11], a taxonomy of channel link quality techniques is presented providing a valuable survey on LQEs and asserting importance of link quality estimation in IWSs. In [12], failure analysis and wireless network troubleshooting are performed whenever the CPS is not functioning properly. Interference analysis is one major part of the troubleshooting procedure which is performed through traffic patterns and wireless spectrum analysis. Also, in [13], the use of spectrum analysis for interference detection and estimation is proposed for IWSs.

LQE is one important but insufficient aspect of assessing the impact of link quality on a CPS. We assert that by jointly observing the performance of the physical and wireless components of a CPS, one obtains the complete perspective of the quality of the wireless link and its impact on physical performance. Since interference is such an important topic in the wireless CPS, we are motivated to contribute a method that simultaneously (1) makes observations of the physical system using ground truth measurements, and (2) infers the quality of the wireless communication system in terms of signal-to-interference ratio (SIR) using a relevant use case found in industry.

In this paper, we present a method using random forest regression to estimate the SIR ratio of the communication channel within a robotic arm force-seeking scenario in which the force signal is transmitted over a wireless local area network (WLAN) [14]. Position data from a vision-based tracking system, a distant observer, is used to train a channel quality estimator to infer the SIR of the wireless channel. The experiment is designed so that the small perturbations in the wireless channel resulting from interference will present position uncertainty in the physical system.

Our paper is organized as follows: In Section II the use case is presented with details of its construction. In Section III we present our process of data collection and subsequent analysis to include statistical exploration and our machine learning approach. We then present the results of our analysis in Section IV followed by conclusions and future direction in Section V.

II. Robot Arm Force-Seeking Application

A. General Construction and Operation

A robotic force-seeking apparatus is constructed using a Universal Robots UR-3 collaborative robot. As illustrated in Fig. 1, the robot is fitted with a six degrees-of-freedom (DOF) force-torque sensor (FTS) followed by a probe. The robot is programmed to apply a downward force, $F(t)$, in the z direction until a force exceeding a threshold, F_t, is reported to the controller. The robot encounters the force threshold through a fixed plunger-spring assembly. The force in the spring is governed by the equation $F(t) = kl$ where k is the spring constant and l is the spring deflection. The robot will push the spring downward repeatedly for the duration of 30 minutes. Plunger movement is limited by a hard stop which will reset the height of the robot arm. A photograph of the force-seeking apparatus is shown in Fig. 2. The illuminated spheres shown in the photo are infrared markers used by the remote observer to track the position of the probe.

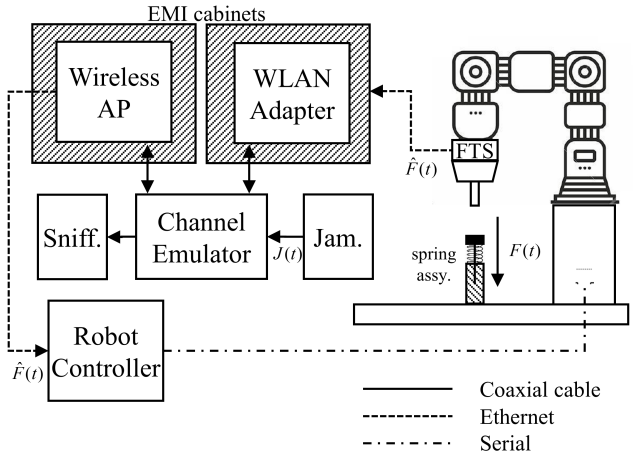

Fig. 1. Robot force-seeking spring system with controlled wireless channel emulation and interference injection.

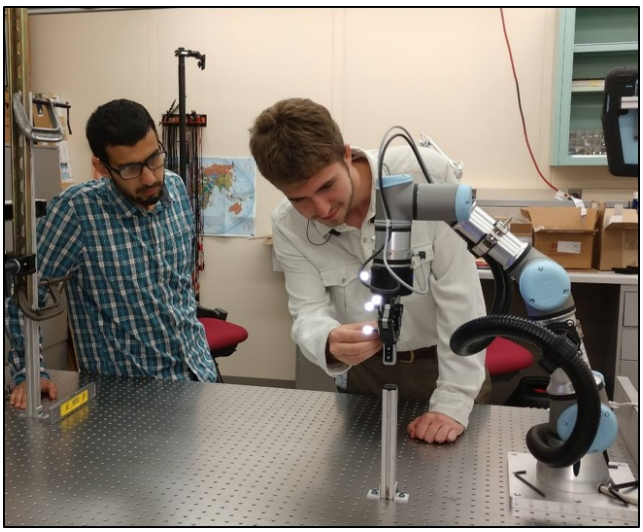

Fig. 2. A photograph of the robot force-seeking experiment shows the robotic arm, the spring-based plunger, and the visual markers used for position tracking.

B. Components

Referring again to Fig. 1, the system is composed of the following components:

Robot The robotic arm applies a downward force along the z-axis to the plunger-spring assembly. The robot is a 6-DOF rigid body manipulator in which all joints have a full 360 degrees of motion. For the experiment, the robot is configured such that it would replicate the action of a robot applying a force to push a small part into place within an automotive assembly work-cell [15]. The robot is mounted on a motionless optics table in which mechanical vibration is dampened.

Robot Controller The robot controller (RC) provides the

motion control function of all joints on the robot. The RC is responsible for controlling motion while searching for a force feedback signal.

Force Torque Sensor The force torque sensor (FTS) provides continuous force and torque readings at a rate of 125 Hz. Readings from the FTS include force measurements in Newtons along the three Cartesian axes, x, y, and z, and three torque readings in Newton-meters (N-m) about each axis. The FTS is designed to communicate with the RC through an Ethernet connection.

Robot End-effector The robot end-effector (REEF) is a rigid body probe attached to the end of the robot arm just after the FTS. The REEF is used to make contact with the plunger-spring assembly.

Wireless Components The wireless Ethernet adapter (WEA) replaces the Ethernet connection between the FTS and the RC with a Wi-Fi connection. The adapter supports the IEEE 802.11 b, g, n, and ac modes. The WEA connects to the RC through a wireless access point (WAP).

Jammer The jammer provides the source of interference, J, which is directly injected into the wireless channel. For simplicity, interference is injected as non-modulated additive white Gaussian noise (AWGN). The power of J at each receiver is determined by its distance to the jammer.

Channel Emulator The channel emulator (CE) provides the capability to control the electromagnetic channel between the WEA and the WAP. The CE supports frequencies between 1 GHz and 6 Ghz and has an instant bandwidth of 250 MHz. It also supports a channel impulse response of 13 taps with a minimum time resolution of 4 ns making the replication of close-quarter multi-path reflections possible. As shown in Fig. 1, all wireless devices are connected to the CE.

Electromagnetic Interference Cabinets The electromagnetic interference (EMI) cabinets provide isolation between devices such that communication between devices does not occur through radiated leakage.

Wireless Sniffer A wireless sniffer (WS) is used to monitor wireless traffic during operation. The sniffer is connected to a laptop computer running Wireshark, and packet logs are used for offline analysis of network events.

Vision Tracking System An OptiTrack VS120 Trio is used as the vision-based tracking system (VTS) to produce accurate ground truth measurements of the probe position. Position estimates along the z-axis are captured at the maximum video frame rate of 120 frames per second. Each estimate includes time and position.

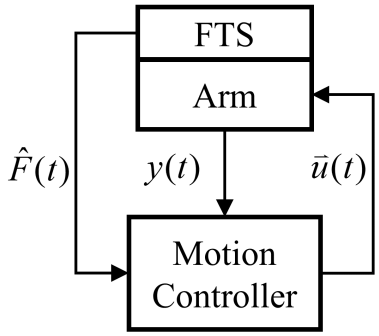

Fig. 3. Feedback signal flow model of the force-seeking controller

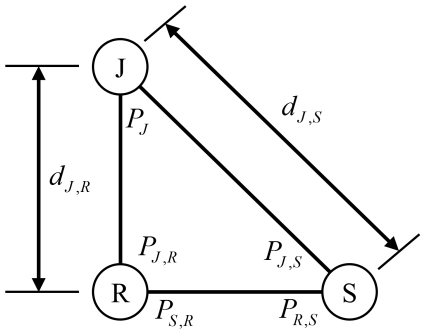

Fig. 4. RF emulation scenario design of the robotic force-seeking scenario.

C. Robot Arm Motion Control

A diagram of the control system for the robotic manipulator is shown in Fig. 3. The UR-3 is constructed of the manipulator assembly and the RC assembly. The internal construction of the robot arm is irrelevant for this experiment, but it is assumed that the arm produces encoder positions $y(t)$ for each joint. It is also assumed that the robot arm accepts actuation signals $\vec{u}(t)$ from the motor drives located in the RC. Both $y(t)$ and $\vec{u}(t)$ are conveyed through wired connections. The force sensor signal $\hat{F}(t)$ is produced by the FTS and is conveyed via an IEEE 802.11 wireless connection. The RC is programmed to move a probe connected to the end of the manipulator downward along a linear path until a force of at least 5 N is detected. The RC will not move the arm during the force-seeking operation unless it receives an FTS signal; therefore, the duration and continuity of the movement of the arm will be impacted by unreliable communication between the FTS and the RC.

D. RF Emulation Scenario

The CE is programmed using a graphical user interface in which the wireless scenario is modeled. Scenarios are composed of radios, platforms, and links. Platforms represent

the physical machine on which a radio may be deployed. Platforms may be mobile or stationary, ground-based or aerial. Radios are assigned to platforms, and each radio is associated to a physical port on the emulator. Links are representations of the physical connections between radios. Each link has an associated path loss and multi-path representation. Path loss is implemented according to Friis equation [16] simplified as $P_r = P_t + C - 10\gamma \log_{10}(d)$, where P_r is the received power, P_t is the transmitted power, C is a characteristic constant representing characteristics of the channel and electronics, γ is the path loss exponent, and d is the distance between transmitter and receiver. For simplicity, we assume that path loss occurs in accordance with the square of the distance ($\gamma = 2$); however, in practice, the path loss exponent is usually greater, causing a more rapid loss of signal power over the same distance [17]. Since the focus of this work is to infer signal quality from ground truth measurements, the path loss exponent is inconsequential to our analysis.

Shown in Fig. 4 is the general scenario for the wireless communication system employed for the force feedback control system. In the figure, there are three nodes, a wireless router (R), a wireless station (S), and a jammer (J). The router and station transmit with nominal power that is dependent upon the 802.11 protocol. The jammer transmits with constant power, and its impact on the scenario depends on its position relative to the other nodes. The distance between J and R is denoted by $d_{J,R}$, and the distance between the J and S is denoted by $d_{J,S}$. The resulting signal-to-interference power ratio (SIR) for the router is defined in decibels as $SIR_{J,R} = P_{S,R} - P_{J,R}$ which is the power received by the router of the station signal divided by the power of interference experienced at the router. Similarly, the SIR experienced at the station is defined as $SIR_{J,S} = P_{R,S} - P_{J,S}$ which is the received signal power of the router at the station divided by the interference power experienced at the station.

For each experiment, the location of the J is adjusted to produce a desired SIR. Each time the location of J is changed, the robot is allowed to operate for a period of 30 minutes. This included periods of inaction by the robot when the SIR prohibits movement of the arm. The SIR setting was validated for each run using a real-time spectrum analyzer connected directly to the emulator.

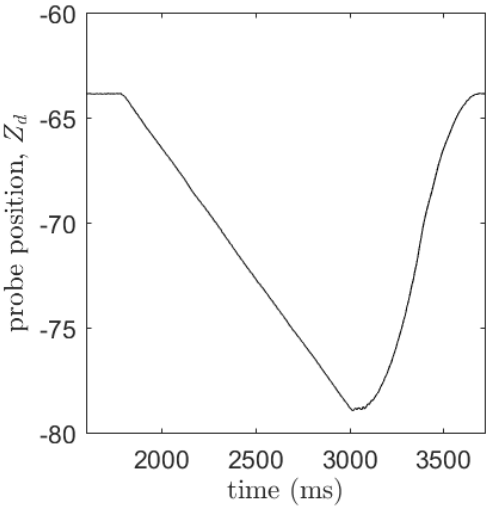

(a) sample time series of probe position

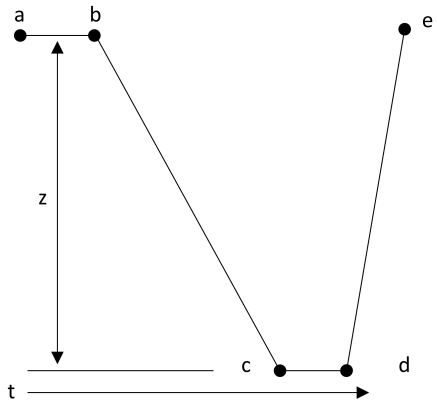

(b) feature extraction model

Fig. 5. A time-series sample (a) of a single iteration of the measured z-axis probe position and (b) the corresponding model for feature extraction.

III. Data Analysis

The data analysis process for the experiment is divided into four parts: raw data collection, data cleaning and feature extraction, training, and the operation of the SIR estimation. The raw data was produced as an output of the VTS as a time series of z-axis position. Feature extraction was conducted in MATLAB by following the time series and extracting or calculating features for each iteration. Once features were extracted, a statistical analysis of the features was conducted to determine the variability of the features as a function of SIR. Statistical analyses included visual inspection of histograms of each factor and an inspection of the correlation coefficients over the range of SIRs. A discussion of the statistical results is provided in IV-A which demonstrates suitability of the use of position measurements for machine learning. Training of a machine learning algorithm followed. The machine learning algorithm was programmed in Python using the Sci-kit Learn library [18].

A. Feature Extraction

Feature extraction begins with a time series of position of the probe through successive iterations of the plunger applying force to the spring and then returning to its home position. A sample time series of the z-axis position of the probe is as shown in Fig. 5a. Rather than using the time series directly, a more convenient and practical solution is to extract features that represent aspects that may be useful for analysis and machine learning algorithms. This reduces the number of learning dimensions and usually improves computation efficiency. The selected features are illustrated in Fig. 5b. Shown in the model, the probe begins at its home position, **a**. It will not begin its downward motion until it receives sufficient FTS readings. Marker **b** indicates the beginning of the probes descent. Marker **c** represents that point in which the probe descends below a predetermined threshold, and marker **d** represents the position in which the probe begins its return ascent to the home position. Finally the probe returns to the home position as indicated by marker **e**. Therefore, the extracted features of each successive iteration is defined as follows:

Feature Z_d The length of the probe's descent measured in millimeters,

Feature Δt_{ab} The duration in seconds the the robot waits before moving the probe along its descent,

Feature Δt_{bc} The duration in seconds of the time that the robot takes to move the probe beyond the threshold, Z_{th}, of -77 mm,

Feature Δt_{cd} The duration in which the probe dwells below Z_{th} and the speed of the probe remains under 0.15 mm/sec,

Feature Δt_{ae} The duration of the full iteration as measured from the home position, **a**, to the next home position, **e**.

B. Statistical Analysis

Each factor was visually examined to assess its variability as a function of the SIR. In order to predict the SIR given a set of measurements of the dynamics of the physical system, sufficient variability is needed. This assessment was performed visually using histograms as a basis for comparison. The factors Z_d and Δt_{bc} were used for examination of the data using histograms.

In addition, it would be helpful to show that the factors are uncorrelated as a function of SIR demonstrating a further level of confidence that each factor will be useful to a machine learning algorithm. This assessment was accomplished by computing the correlation coefficient matrix of the extracted factors as defined by the Pearson product-moment method [19]. The correlation coefficient matrix is a covariance matrix that is normalized by the product of the standard deviations of two factors being compared according to $\rho_{X,Y} = cov(X,Y)/(\sigma_X \sigma_Y)$. Since each factor correlates exactly with itself, a correlation matrix should have values of 1 along the diagonal. Other elements of the matrix will take on values between -1 and 1. A visual inspection of the coefficient matrices will show how strongly selected factors vary together. Correlation can be viewed as a function of SIR to verify that factors are independently applicable to a learning algorithm. The objective of factor selection is, therefore, to choose factors that are highly uncorrelated and yet still vary appreciably [20].

C. Machine Learning

In order to learn the SIR level from observing the various features, we leverage the random forest model [21]. Random forest is an ensemble of decision trees with random feature selection which can be used for classification or regression based on the predicted output space. Deploying random forest in machine learning has been successful in various applications such as [22]–[24]. Its main advantages are that it is stable, fast to compute, and insusceptible to over-fitting.

In this work, we deploy the random forest model for SIR regression using the five features defined in III-A. These features are evaluated for each iteration of the probe movement. We define a data segment which is composed of a number of successive iterations and we denote the segment size by M. As a result, we use the random forest regression model to get an input vector of size $5M$ and regression output of the corresponding SIR value. The random forest is selected because it is computationally efficient with high-dimensional data and it is robust for outliers and data non-linearity.

We start by training the random forest regression model by taking a fixed number of segments for each SIR labelled data. We denote the size of the training set for each SIR level by T. The rest of the measurements are used for testing. In general, the proposed machine learning approach will deploy a sliding window approach of size M to collect the features of the force-seeking use case to estimate the current level of SIR at various nodes of the wireless network.

IV. Results

The results in this section are presented from an experimental run in which the jammer **J** interferes with the router, **R**, while communication is conducted using a mixed mode of IEEE 802.11 b and g [14]. Analyses using histograms and covariance are presented in Section IV-A followed by results of the machine learning application in Section IV-B.

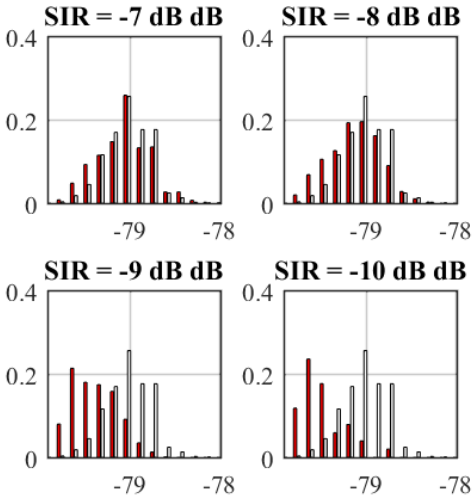

(a) z-axis position

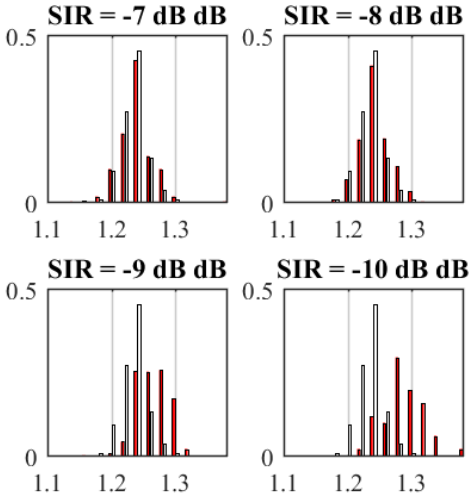

(b) Plunge delay Δt_{bc}

Fig. 6. Variations in probability distributions of the z-axis position (a) and the plunge delay (b) indicate that machine learning may be effective in inferring information about the underlying communication channel. In the figure, the baseline case of infinite SIR is depicted as a histogram with white bars, and the experimental case is depicted as a histogram with red bars.

A. Statistical Analysis

1) Analysis of Factors Using Histograms: The results of the histogram analyses for the z-axis position of the probe and the probe descent delay are shown in Fig. 6a and Fig. 6b, respectively. The expectation of the histogram analysis was that Z_d and the ΔT_{bc} would exhibit appreciable variation that may be observed through a visual inspection. This was indeed the case. Referring to Fig. 6a, a visual inspection reveals that the minimum z-axis position for each iteration skews to lower positions for lower SIR values and higher positions for higher SIR values. This implies that the controller algorithm responds faster to force sensor readings at higher SIR values than lower values. Similarly, by observing the plunge delay, Δt_{bc}, the controller takes more time to respond at lower SIR values than at higher values. This behavior is exemplified by the probability skew shown in the histograms.

TABLE I
CORRELATION COEFFICIENTS FOR $-9\ dB$ SIR

	Δt_{ab}	Δt_{bc}	Z_d	Δt_{cd}	Δt_{ae}
Δt_{ab}	1	0.04	0.04	0	0.56
Δt_{bc}	0.04	1	-0.96	-0.08	0.18
Z_d	0.04	-0.96	1	0.03	-0.01
Δt_{cd}	0	-0.08	0.03	1	0
Δt_{ae}	0.56	0.18	-0.01	0	1

TABLE II
CORRELATION COEFFICIENTS FOR $-8\ dB$ SIR

	Δt_{ab}	Δt_{bc}	Z_d	Δt_{cd}	Δt_{ae}
Δt_{ab}	1	0.01	-0.05	-0.06	0.58
Δt_{bc}	0.01	1	-0.99	-0.13	0.1
Z_d	-0.05	-0.99	1	0.07	-0.1
Δt_{cd}	-0.06	-0.13	0.07	1	-0.03
Δt_{ae}	0.58	0.1	-0.1	-0.03	1

TABLE III
CORRELATION COEFFICIENTS FOR $-7\ dB$ SIR

	Δt_{ab}	Δt_{bc}	Z_d	Δt_{cd}	Δt_{ae}
Δt_{ab}	1	-0.05	-0.04	0.09	0.01
Δt_{bc}	-0.05	1	-0.93	-0.17	0.05
Z_d	-0.04	-0.93	1	0.08	-0.05
Δt_{cd}	0.09	-0.17	0.08	1	-0.02
Δt_{ae}	0.01	0.05	-0.05	-0.02	1

2) Factor Correlation Coefficient Analysis: Correlation coefficients were calculated for each of the five factors defined in Section III-A and correlation coefficients matrices were produced for each of the SIR values used. The correlation coefficient matrices for SIR values of -9, -8, and -7 are shown in Tables I-III, respectively. Inspection of the correlation coefficient tables indicate that the factors are mostly uncorrelated across SIR values except for the clear correlation between plunge delay and plunge depth. Low correlation values demonstrate a necessary but not sufficient condition for the independent applicability factors to machine learning. If desired, either Δt_{bc} or Z_d could be omitted as they are strongly correlated and therefore provide redundant information.

B. Machine Learning Results

We deploy the proposed machine learning approach to three values of the SIR, -9, -8, and -7 dB. We start by showing the output of the random forest regression model for two values

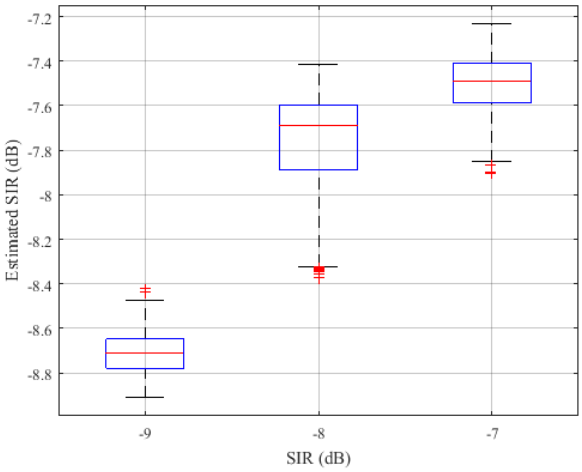

(a) $M = 100$

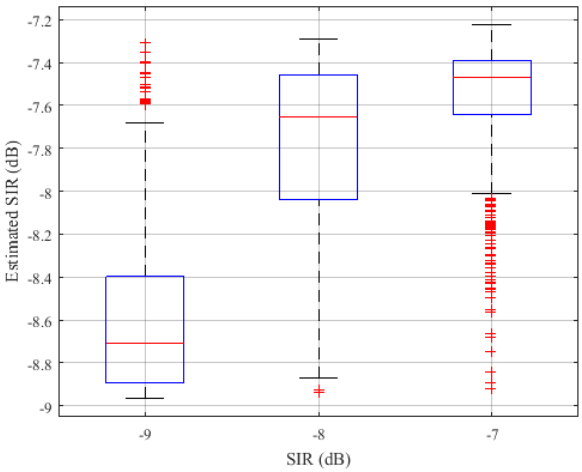

(b) $M = 1$

Fig. 7. Predicted SIR versus actual SIR for the cases of (a) $M = 100$ and (b) $M = 1$. The box plots show the median value while the bottom and top edges of the box indicate the 25th and 75th percentiles. Statistical outliers are shown as red $+$ signs.

of the segment size M. We set the training set size $T = 200$ for each SIR value. We use the random forest model with a number of estimators of 500 and a tree depth of 5. In Fig. 7, we present the box plots of the predicted SIRs against the correct value of the corresponding SIR for $M = 100$ and $M = 1$. Generally, increasing the value of M increases the acquisition time for the input data for the random forest model while enhancing the performance of the algorithm. By setting $M = 1$, we notice that the predicted values of SIR are widely spread around the median and a large number of outliers exists. However, by increasing M, we have much less variations in the predicted SIRs and a smaller number of outliers.

In Fig. 8, we present the two criteria for measuring the

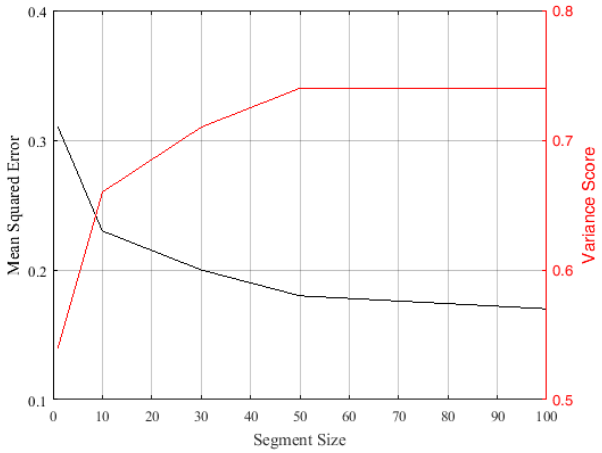

Fig. 8. The performance of the random forest regression model against M.

performance of the proposed SIR estimation algorithm. We show the performance against the segment size M. The first criterion is the mean squared error where the mean of the squared error between the estimated SIR and the actual SIR values is calculated. The second criterion is the variance score which is a statistical measure of how close the data are to the fitted regression line. We use the r-squared variance score that is defined as the ratio between the total variance explained by model and total variance of the data [25]. In this figure the improvement in the performance against the segment size is demonstrated.

V. Conclusion

In this paper we have presented a practical use case of a wireless force-torque feedback control system that could be deployed in a manufacturing assembly system such as a pick-and-place or assembly operation. A 6-DOF force sensor was connected to a robot controller tasked with moving a probe along a linear path until an opposing force exceeding 5 N was detected. We demonstrated that the reliability of the wireless communication system directly impacts the repeatability performance of the physical system. We also demonstrated that the quality of the underlying wireless channel may be inferred by observing the position of the probe along a single spatial dimension and applying machine learning to predict the signal-to-interference ratio. Our findings provide motivation for applying machine learning to larger more complex systems with high degrees of freedom. Future work will extend to the inclusion of more descriptive factors, the addition of network information such as the wireless protocol mode, and the addition of a larger number of variables tracked by many remote observers. Experimentation with neural networks

and deep learning to improve prediction accuracy and better generalization will be of great values to wireless operations in factories. Finally, the applications of online machine learning techniques to this and other use cases could provide significant benefits to the manufacturing community.

DISCLAIMER

Certain commercial equipment, instruments, or materials are identified in this paper in order to specify the experimental procedure adequately. Such identification is not intended to imply recommendation or endorsement by the National Institute of Standards and Technology, nor is it intended to imply that the materials or equipment identified are necessarily the best available for the purpose.

REFERENCES

[1] R. Candell, M. Hany, K. B. Lee, Y. Liu, J. Quimby, and K. Remley, "Guide to industrial wireless systems deployments," National Institute of Standards and Technology, Gaithersburg, MD, Tech. Rep., Apr 2018. [Online]. Available: http://nvlpubs.nist.gov/nistpubs/ams/NIST.AMS.300-4.pdf

[2] E. Sisinni, A. Saifullah, S. Han, U. Jennehag, and M. Gidlund, "Industrial Internet of Things: Challenges, Opportunities, and Directions," *IEEE Transactions on Industrial Informatics*, 2018.

[3] L. L. Bello, J. Åkerberg, M. Gidlund, and E. Uhlemann, "Guest Editorial Special Section on New Perspectives on Wireless Communications in Automation: From Industrial Monitoring and Control to Cyber-Physical Systems," *IEEE Transactions on Industrial Informatics*, vol. 13, no. 3, pp. 1393–1397, 2017.

[4] Z. Pang, M. Luvisotto, and D. Dzung, "Wireless High-Performance Communications: The Challenges and Opportunities of a New Target," *IEEE Industrial Electronics Magazine*, vol. 11, no. 3, pp. 20–25, 2017.

[5] R. Candell, "Industrial wireless systems workshop proceedings," National Institute of Standards and Technology, Gaithersburg, MD, Tech. Rep., May 2017. [Online]. Available: https://nvlpubs.nist.gov/nistpubs/ir/2017/NIST.IR.8174.pdf

[6] C. Lu, A. Saifullah, B. Li, M. Sha, H. Gonzalez, D. Gunatilaka, C. Wu, L. Nie, and Y. Chen, "Real-Time Wireless Sensor-Actuator Networks for Industrial Cyber-Physical Systems," *Proceedings of the IEEE*, vol. 104, no. 5, pp. 1013–1024, May 2016. [Online]. Available: http://ieeexplore.ieee.org/document/7348717/

[7] D. Kim, Y. Won, Y. Eun, and K.-J. Park, "W-Simplex: Resilient network and control co-design under wireless channel uncertainty in cyber-physical systems," in *2017 IEEE Conference on Control Technology and Applications (CCTA)*. IEEE, Aug 2017, pp. 49–54. [Online]. Available: http://ieeexplore.ieee.org/document/8062439/

[8] T. M. Chiwewe, C. F. Mbuya, and G. P. Hancke, "Using Cognitive Radio for Interference-Resistant Industrial Wireless Sensor Networks: An Overview," *IEEE Transactions on Industrial Informatics*, vol. 11, no. 6, pp. 1466–1481, Dec 2015. [Online]. Available: http://ieeexplore.ieee.org/document/7299315/

[9] N. Bhushan, Junyi Li, D. Malladi, R. Gilmore, D. Brenner, A. Damnjanovic, R. Sukhavasi, C. Patel, and S. Geirhofer, "Network densification: the dominant theme for wireless evolution into 5G," *IEEE Communications Magazine*, vol. 52, no. 2, pp. 82–89, Feb 2014. [Online]. Available: http://ieeexplore.ieee.org/document/6736747/

[10] R. D. Gomes, D. V. Queiroz, A. C. Lima Filho, I. E. Fonseca, and M. S. Alencar, "Real-time link quality estimation for industrial wireless sensor networks using dedicated nodes," *Ad Hoc Networks*, vol. 59, pp. 116–133, May 2017. [Online]. Available: https://linkinghub.elsevier.com/retrieve/pii/S1570870517300434

[11] N. Baccour, A. Koubâa, L. Mottola, M. A. Zúñiga, H. Youssef, C. A. Boano, and M. Alves, "Radio link quality estimation in wireless sensor networks," *ACM Transactions on Sensor Networks*, vol. 8, no. 4, pp. 1–33, Sep 2012. [Online]. Available: http://dl.acm.org/citation.cfm?doid=2240116.2240123

[12] U. Wetzker, I. Splitt, M. Zimmerling, C. A. Boano, and K. Romer, "Troubleshooting Wireless Coexistence Problems in the Industrial Internet of Things," in *Proceedings - 19th IEEE International Conference on Computational Science and Engineering, 14th IEEE International Conference on Embedded and Ubiquitous Computing and 15th International Symposium on Distributed Computing and Applications to Business, Engi*, 2017.

[13] G. H. Koepke, W. F. Young, J. M. Ladbury, and J. B. Coder, "Interference and Coexistence of Wireless Systems in Critical Infrastructure," National Institute of Standards and Technology, Gaithersburg, MD, Tech. Rep., Jul 2015. [Online]. Available: https://nvlpubs.nist.gov/nistpubs/TechnicalNotes/NIST.TN.1885.pdf

[14] IEEE Standards Association, *Part 11: Wireless LAN Medium Access Control (MAC) and Physical Layer (PHY) Specifications; Amendment 4: Enhancements for Very High Throughput for Operation in Bands below 6 GHz*, 2013.

[15] M. L. T. Cossio, L. F. Giesen, G. Araya, M. L. S. Pérez-Cotapos, R. L. VERGARA, M. Manca, R. A. Tohme, S. D. Holmberg, T. Bressmann, D. R. Lirio, J. S. Román, R. G. Solís, S. Thakur, S. N. Rao, E. L. Modelado, A. D. E. La, C. Durante, U. N. A. Tradición, M. En, E. L. Espejo, D. E. L. A. S. Fuentes, U. A. D. Yucatán, C. M. Lenin, L. F. Cian, M. J. Douglas, L. Plata, and F. Héritier, *Springer Handbook of Robotics*, B. Siciliano and O. Khatib, Eds. Springer International Publishing, 2016. [Online]. Available: http://link.springer.com/10.1007/978-3-319-32552-1

[16] J. A. Shaw, "Radiometry and the Friis transmission equation," *American Journal of Physics*, vol. 81, no. 1, pp. 33–37, Jan 2013. [Online]. Available: http://aapt.scitation.org/doi/10.1119/1.4755780

[17] R. Candell, C. Remley, J. Quimby, D. Novotny, A. Curtin, P. Papazian, G. Koepke, J. Diener, and M. Kashef, "Industrial wireless systems: Radio propagation measurements," National Institute of Standards and Technology, Gaithersburg, MD, Tech. Rep., 2017. [Online]. Available: http://nvlpubs.nist.gov/nistpubs/TechnicalNotes/NIST.TN.1951.pdf

[18] "scikit-learn: machine learning in Python." [Online]. Available: http://scikit-learn.org/stable/

[19] K. Yeager, "LibGuides: SPSS Tutorials: Pearson Correlation." [Online]. Available: https://libguides.library.kent.edu/SPSS/PearsonCorr

[20] J. Lee Rodgers and W. Alan Nice Wander, "Thirteen ways to look at the correlation coefficient," *American Statistician*, pp. 59–66, 1988.

[21] L. Breiman, "Random forests," *Machine Learning*, vol. 45, no. 1, pp. 5–32, Oct 2001. [Online]. Available: https://doi.org/10.1023/A:1010933404324

[22] X. Zhen, Z. Wang, M. Yu, and S. Li, "Supervised descriptor learning for multi-output regression," in *2015 IEEE Conference on Computer Vision and Pattern Recognition (CVPR)*, June 2015, pp. 1211–1218.

[23] J. Shotton, A. Fitzgibbon, M. Cook, T. Sharp, M. Finocchio, R. Moore, A. Kipman, and A. Blake, "Real-time human pose recognition in parts from single depth images," in *CVPR 2011*, June 2011, pp. 1297–1304.

[24] X. Zhen, Z. Wang, A. Islam, M. Bhaduri, I. Chan, and S. Li, "Direct estimation of cardiac bi-ventricular volumes with regression forests," in *Medical Image Computing and Computer-Assisted Intervention – MICCAI 2014*, P. Golland, N. Hata, C. Barillot, J. Hornegger, and R. Howe, Eds. Cham: Springer International Publishing, 2014, pp. 586–593.

[25] S. Deb, "A novel robust r-squared measure and its applications in linear regression," in *Computational Intelligence in Information Systems*, S. Phon-Amnuaisuk, T.-W. Au, and S. Omar, Eds. Cham: Springer International Publishing, 2017, pp. 131–142.